International Journal of Rotating Machinery, 7(6): 425–433, 2001

1023-621X/01 $12.00 + .00

Effects of Gaps Between Side-Walls and 60° Ribs on the Heat Transfer and Rib Induced Secondary Flow Inside a Stationary and Rotating Cooling Channel

Robert Kiml, Sadanari Mochizuki, and Akira Murata
Tokyo University of Agriculture & Technology, Department of Mechanical Systems Engineering, Tokyo, Japan

The present study investigates the effects of gaps between the side-walls and 60° ribs on the local heat transfer distribution between two consecutive ribs. The heat transfer and flow visualization experiments were carried out inside a straight rib-roughened duct with the ribs mounted on two opposite side walls with and without the gaps. The results showed that the existence of the gaps appreciably enhances the *Nu* in the area between two consecutive ribs. It is caused by (1) the introduction of the fresh air through the gaps into this region, and (2) the improvement of the three-dimensional flow structure in the area between the two ribs.

Keywords Forced convention, Secondary flow, Flow separation, Internal cooling of gas turbines, Particle tracer method, Ribs

INTRODUCTION

Among numerous heat transfer enhancement techniques, ribs are widely employed to augment the heat transfer performance inside cooling passages of gas turbine blades (see Fig. 1). The mechanism of heat transfer enhancement by the conventional ribs is based on the flow separation and reattachment as can be well demonstrated by the transverse ribs that induce basically two-dimensional flow phenomenon.

When heat is transferred from the wall to the flowing fluid inside a cooling passage, fluid temperature in the core region is always lower than that near the wall. Therefore, if the cold and higher momentum fluid in the central core region of the channel is by some means carried to the hot area near the wall, heat transfer will be enhanced. In other words, if the secondary flow occurs, the thickness of both velocity and thermal boundary layers on the wall where the flow from the tube core region hits will become thinner and the heat transfer in that region will be augmented. In order to do that, a lot of time has been devoted to a development of an optimal rib configuration, which could augment the heat transfer appreciably and consequently enhance the efficiency of the gas turbine engine.

For example, studies by Han (1984), Han et al. (1985), Rau et al. (1996), Kiml et al. (2000) and Mochizuki et al. (1997) studied the heat transfer and pressure characteristics in rib-roughened passages with different rib arrangements. They focused on the effects of the Reynolds number and rib geometry on the heat transfer and pressure drop in the fully developed region of a uniformly heated square and rectangular channels. All these studies also showed that the secondary flow induced by the rib inclination augment the heat transfer better than the transverse ribs. Further studies by Johnson et al. (1993), Taslim et al. (1991), Dutta et al. (1996), Wagner et al. (1992) and El-Husayni et al. (1994) examined the effects of Coriolis forces, centrifugal force, and buoyancy force on the heat transfer characteristics with different rib configurations. The effects of the 180° sharp turn on the flow, pressure drop, and heat transfer in a serpentine passage have been reported by Cheng et al. (1992), Chneg and Shi (1996), Metzger et al. (1984) and Kiml et al. (1998). Studies by Taslim et al. (1994), Dutta et al. (1995), Hu and Shen (1996), Han et al. (1991–1992), Ekkad and Han (1997), Kawaike et al. (1995), and Johnson et al. (1993) presented the heat transfer results for the parallel, broken, crossed, and V-shaped rib patterns. However, with the advancement of gas turbine technology it became necessary to focus attention on more details, which could augment the heat transfer even further.

The present study focuses on the detailed examination of the influence of gaps (between the 60° ribs and side walls) on the local heat transfer distribution and flow behavior inside a straight rib-roughened duct. The emphasis was especially placed

Received in final form 12 July 2001.
The authors would like to express their gratitude to Mr. T. Takahashi and S. Takeda, who were very helpful in carrying out the experiments.
Address correspondence to Dr. Robert Kiml, Tokyo University of Agriculture & Technology, Department of Mechanical Systems Engineering, Nakacho 2-24-16, Koganei-shi, Tokyo 184-8588, Japan. E-mail: robert@mmlab.mech.tuat.ac.jp

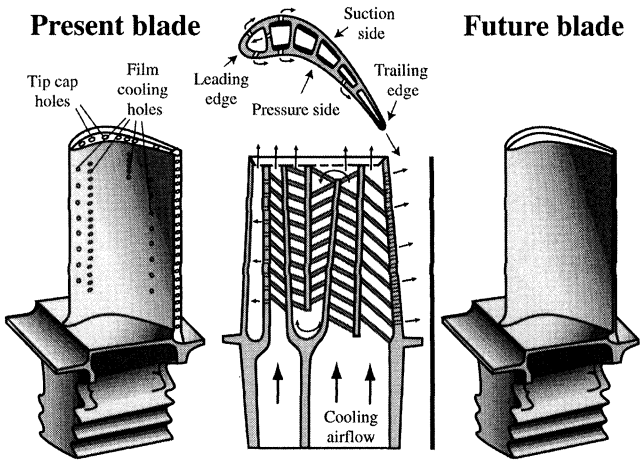

FIGURE 1
Schematic of an internal and external structure of a gas turbine blade.

on the exploration of a phenomenon, which has been initially discovered by the present authors for 90° ribs (Kiml et al., 2000). The flow visualization and heat transfer experiments have been carried out for the 60° ribs with (1) NG-No Gaps, (2) SG-Small Gaps, and (3) BG-Big Gaps between the side-walls and ribs.

EXPERIMENTAL APPARATUS AND PROCEDURE

Heat Transfer Experiment

Heat transfer experiments were performed in a straight rib-roughened duct with a square cross section (14 × 14 mm, d_h = 14 mm) and length of 140 mm, as shown in Fig. 2. The test section was attached to a rotating arm and connected to a straight entrance region, with length of 660 mm, which had a rectangular flow cross section identical to the flow passage inside the test section. It was constructed from 5 mm thick Bakelite plates due to its low thermal conductivity, high mechanical strength, and easy machining. The inside surfaces of the test section were covered with thin electric-conductive plastic films, which consist of 180 μm thick polyethylene (PET) layer and a 20 μm thick conductive layer. Uniform wall heat flux conditions were achieved by passing an electric current through the conductive layer of the film. The test section was insulated by 20 mm thick layer of an insulation material SAN PERKA with a heat conductivity of 0.0417 W/(mK). The wall surface temperature was measured by means of 280 K-type thermocouples with a diameter of 50 μm (see Fig. 2). The thermocouples were located in three lines on the ribbed walls and in one line at the center of the side walls. Air temperature at the inlet to the test section was measured by means of four K-type thermocouples (0.3 mm in diameter). The mean bulk outlet temperature was measured by means of 17 thermocouples behind a flow mixing device installed at the exit of the test section.

The measurements were carried out for the 60° ribs, made of Bakelite, with a square cross section (rib-height $h = 1.4$ mm), mounted on the two opposite duct walls with (1) No Gaps, (2) Small Gaps, and (3) Big Gaps between the side-walls and ribs. The gap-size to rib-height ratio was (1) 0, (2) 0.33, and (3) 1, respectively. The Reynolds number varied from Re = 10,000 to 20,000.

To make a performance comparison among the walls of the duct under rotating conditions they were given names:

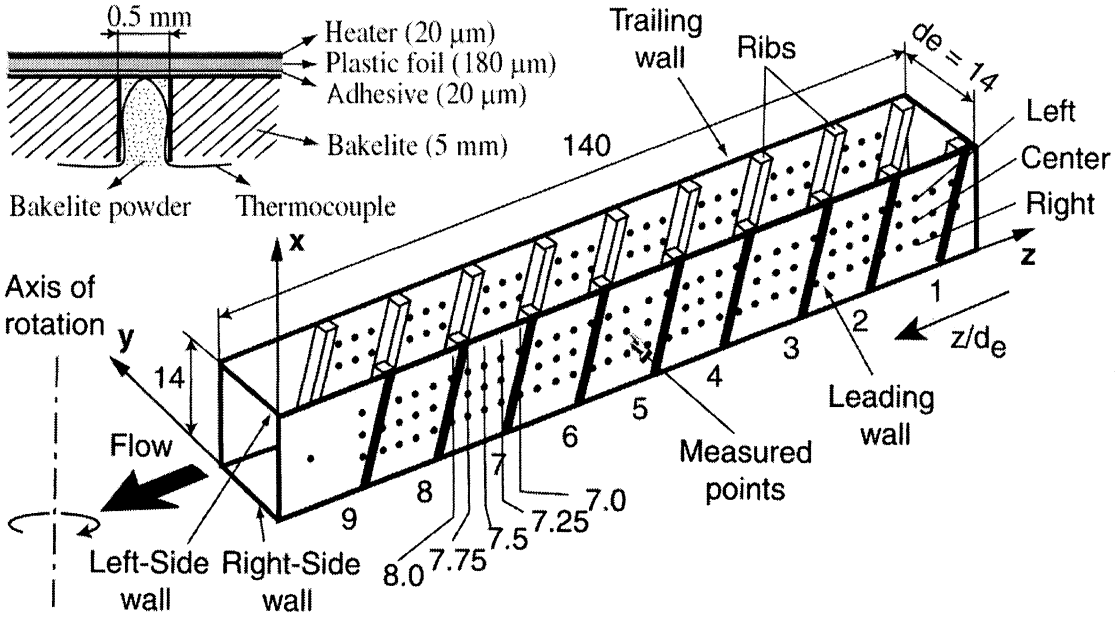

FIGURE 2
Schematic of the heat transfer test section.

"Leading", "Trailing", "Left-Side", and "Right-Side" wall relative to the rotating direction, as shown in Fig. 2.

Flow Visualization Experiment

The experiments were conducted in a test section with a square cross section (150 × 150 mm) made of 10 mm thick transparent Plexiglas plates. The test section was located 5 m downstream of the settling chamber with a free surface on the top. The water level was controlled and maintained at 75 mm (d_h = 150 mm) from the bottom. This was made with the knowledge that the flow behavior inside the channel is symmetrical due to the identical rib arrangement on both rib-roughened walls. Geometric proportions of the ribs, gaps, and Reynolds number were identical with those used in corresponding heat transfer experiments. The 60° ribs with a square cross section (15 × 15 mm^2) were made out of the transparent Plexiglas and mounted on the bottom of the channel, as illustrated in Fig. 3. Three types of rib configurations identical to the heat transfer experiment were used, but only results from the two mostly distinguished rib patterns with: (1) NG-No Gaps and (2) BG-Big Gaps between the side-walls and ribs are presented in this study.

The flow visualization was conducted under stationary conditions using the particle tracer method, between the 4th and 5th ribs where the flow was fully developed. Water was mixed with the chemical compound $NaSO_4$, which increased the specific weight of the water, so that the particles (about 70 μm in diameter) had the same specific weight with that of water. They were illuminated by an argon laser light sheet (3 mm thick) and photographed by a still digital camera and video camera. The camera exposure time was set to 0.5 second to allow the particles

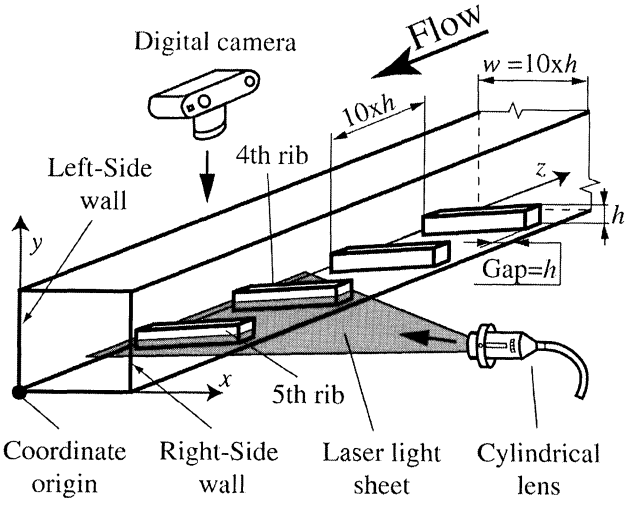

FIGURE 3
Schematic of flow visualization performed by particle tracer method.

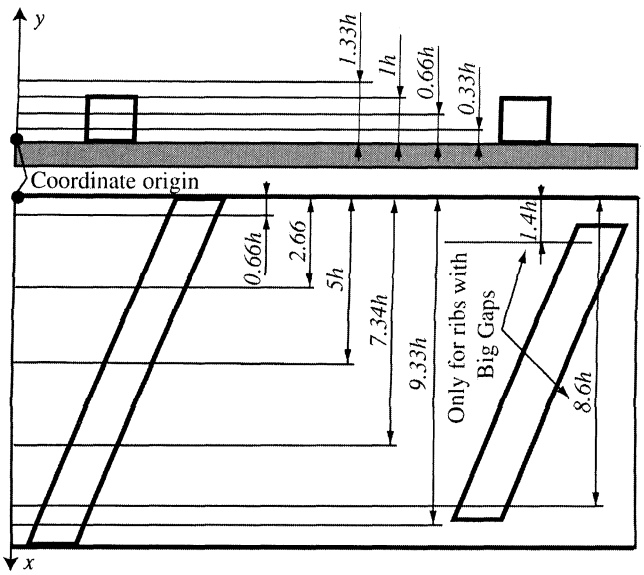

FIGURE 4
Locations where the top and side view patterns were taken.

to create path lines. Top view flow patterns were photographed at four locations $y = 0.33h$; $0.66h$; $1h$; and $1.33h$ from the bottom, as depicted in Fig. 4. Side view patterns were taken at five locations, $x = 9.33h$ (near the Right-side wall region), $7.33h$, $5h$ (center); $2.66h$ and $0.66h$ (near the Left-side wall region) from the Left-side wall plus two more locations in the case of Big Gaps $x = 1.4h$ and $8.6h$ (see Fig. 4).

DATA REDUCTION

The Reynolds number, Rayleigh number, rotational number, wall heat flux, local heat transfer coefficient and Nusselt numbers were defined, respectively, as follows:

$$Re = u_m d_h / \nu, \quad [1]$$

$$Ra = \frac{R\omega^2 \beta \dot{q}_w d_h^4 Pr\, \dot{q}_w}{k\nu^2}, \quad [2]$$

$$Ro = \omega d_h / u_m,$$

$$\dot{q}_w = \dot{m} c_p (T_{out} - T_{in}) / A_h, \quad [3]$$

$$\alpha = \dot{q}_w / (T_w - T_b), \quad [4]$$

$$Nu = \alpha d_h / k, \quad [5]$$

$$Nu_\infty = 0.022\, Re^{0.8}\, Pr^{0.5}. \quad [6]$$

In order to omit any side effects of the not-fully-developed flow behavior at the entrance to the test section and be able to compare results for different rib arrangement with a relatively high accuracy, the mean Nusselt number between $z/d_e = 7 \sim 8$, Nu_{m7-8}, for both rib-roughened and both smooth walls, Leading,

Trailing and Side walls, respectively, was calculated:

$$\Delta T_{w7-8} = \frac{1}{z_{w8} - z_{w7}} \int_{z_{w7}}^{z_{w8}} (T_w - T_b)\, dz, \qquad [7]$$

$$\alpha_{w7-8} = \frac{\dot{q}_w}{\Delta T_{w7-8}}, \qquad [8]$$

$$Nu_{m7-8} = \frac{\alpha_{w7-8} d_e}{k}. \qquad [9]$$

An uncertainty analysis using the ASME Performance Test Codes (ANSI/ASME PTC 19.1-1985), was carried out for the heat transfer experiment and it was estimated that the maximum uncertainties of the Nusselt number were estimated to be less than 9%, for a Reynolds number larger than 10,000.

RESULTS AND DISCUSSION

It is well known from the previous studies that (1) the angled ribs provide better heat transfer enhancement than the transverse ribs due to the development of the secondary flow (Kiml et al., 2000) and (2) the highest heat transfer should be obtained for the rib angle somewhere between 45° and 60°. Therefore, after examination of the gaps effects on the flow behavior and local heat transfer distribution between two consecutive transverse ribs (Kiml et al., 2000), it was decided to examine more in detail the gaps effects of the 60° ribs with (1) No Gaps, and (2) Big Gaps between the Side walls and ribs. The gap phenomenon, which was initially discovered by the present authors, has not been described anywhere else to authors knowledge and therefore it was not possible to compare the presented results with the other studies.

Flow Visualization Results

No Gaps

Figure 5 shows flow patterns representing the flow behavior between the 4th and 5th 60° ribs with No Gaps between the side-walls and ribs. The creation of a large flow separation behind the 4th rib and flow reattachment between the ribs can be clearly observed in these figures. From the flow reattachment region, the local flow streams proceed along the 5th rib towards the left-side wall due to the rib's inclination. Here, as a result of its encounter with the left-side wall (see Fig. 5(d)) and a similar flow stream induced by the ribs mounted on the opposite rib-roughened wall, the flow turns 180° and flows back towards the opposite right-side wall. This flow behavior causes a development of the secondary flow in a form of two vortices, which carry fluid from the central core region towards the right-side wall, as schematically illustrated in Fig. 6.

Big Gaps

In comparison to the previous case, the flow behavior for the 60° ribs with Big Gaps, presented in Fig. 7 and schematically illustrated in Fig. 8, shows that the flow reattachment previously observed only in the near right-side wall vicinity enlarged up

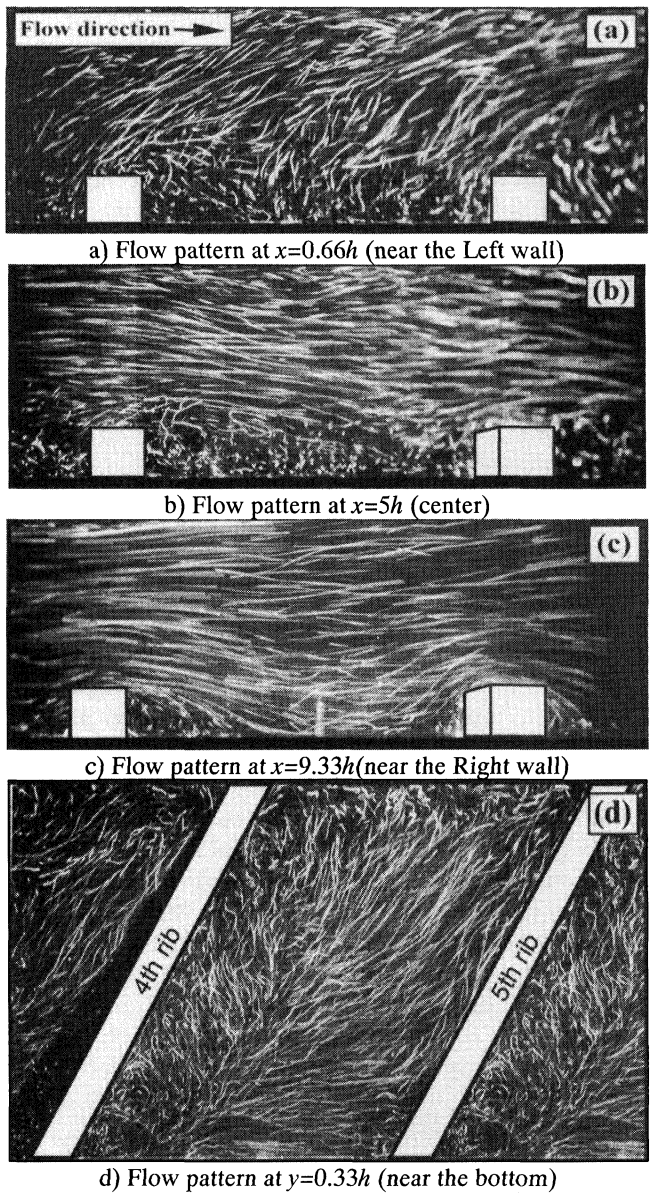

a) Flow pattern at x=0.66h (near the Left wall)

b) Flow pattern at x=5h (center)

c) Flow pattern at x=9.33h(near the Right wall)

d) Flow pattern at y=0.33h (near the bottom)

FIGURE 5
Flow visualization results for 60° ribs with no gaps, $Re = 20{,}000$.

to the channel central region. In addition to that, the size of the flow separation behind the 4th rib diminished (see Fig. (e)) and the flow inside this separation is not circulating as in the previous case, but it is proceeding with a high velocity along this rib. The flow behavior induced by these ribs also creates the secondary flow in the form of two vortices, as was mentioned above, but their rotational momentum is not as strong as it was in the previous case (compare the flow angles in Figs. 7(e) and 5(a). This is caused by a substantial amount of the air proceeding through the gaps between the side walls and ribs, which would be previously forced to hit the side walls and strengthen the vortex rotational momentum.

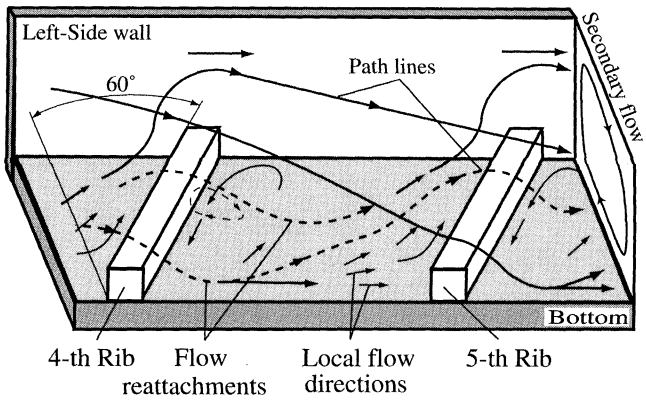

FIGURE 6
Flow pattern between 4th and 5th ribs with no gaps.

Local Heat Transfer Distribution

No Gaps

The local *Nu* distribution between the 7th and 8th 60° ribs with NG in the area just behind the 7h rib is relatively low (see Fig. 9a). This is because the relatively large area is covered by the separated flow. Further from the 7th rib the *Nu*, particularly along the right (▲) and central (●) lines of measurement points, appreciably enhances due to the existence of the flow reattachment at this location. This *Nu* enhancement gradually deteriorates with the increasing distance from the reattachment region due to the boundary layer growth and the flow separation in front of the 8th rib. The boundary layer growth also strongly affects the *Nu* distribution in the near Left wall vicinity (left line (■)) where the lowest *Nu* values between 7th and 8th ribs were obtained.

Big Gaps

The strong gap effects on the local *Nu* distribution at all three lines of measurement points (■, ●, and ▲) can be clearly observed in the case of BG (see Fig. 9(b)). The local *Nu* distribution for this case is generally higher and the local maximum moved from the near right-side wall region to the duct central region. In contrast to the previous case, the significant increase of *Nu* can be seen in the area just behind the 7th rib and along the central line (●) of measurement points, where the local *Nu* maximum also was obtained. It was caused by the existence of a strong flow reattachment which was pushed farther from the right-side wall due to the strong flow stream through the gaps between the right-side wall and ribs (confirm in Fig. 8). In addition to that, the *Nu* deterioration in the main flow direction for this case, along the right (▲) and left (■) lines of measurement points, is not as strong as before. It was caused by a slower boundary layer growth, which was interfered by a strong flow stream from the gaps and almost diminished separation behind or in front of the ribs. This high velocity flow stream from the gaps (near the right-side wall) is also responsible for a significant *Nu* enhancement in the area just in front of the 8th rib (right line (▲)).

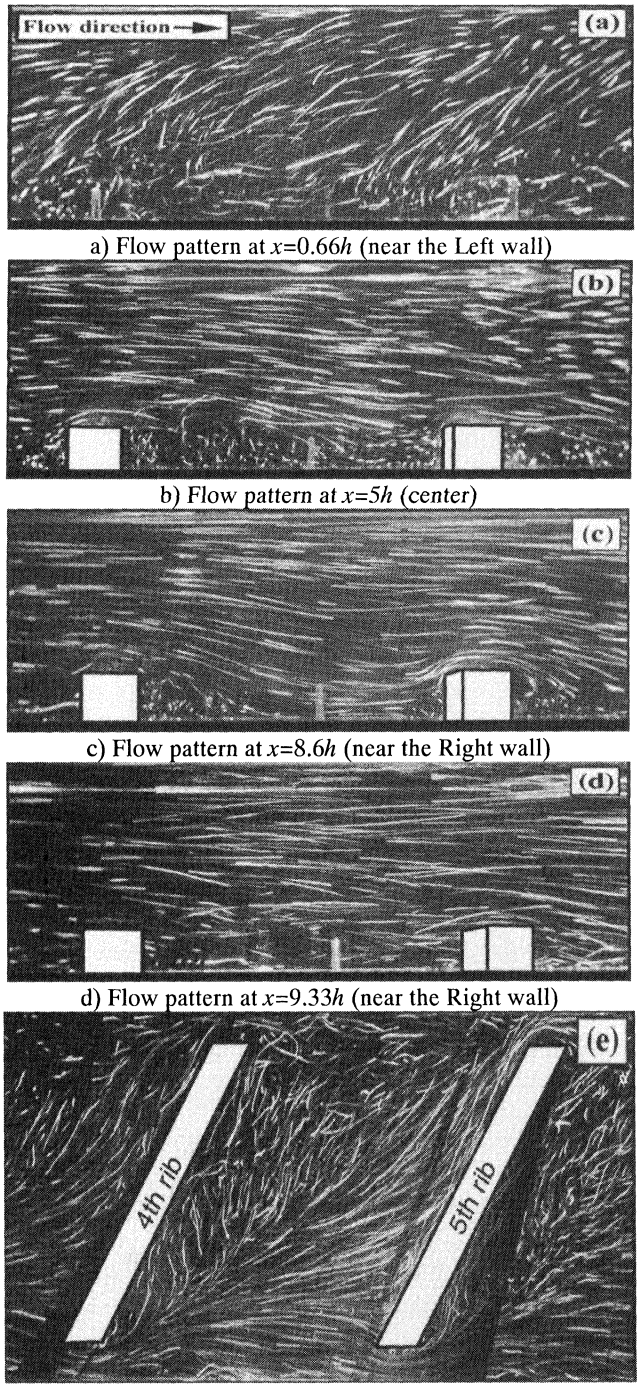

a) Flow pattern at x=0.66h (near the Left wall)

b) Flow pattern at x=5h (center)

c) Flow pattern at x=8.6h (near the Right wall)

d) Flow pattern at x=9.33h (near the Right wall)

e) Flow pattern at y=0.33h (near the bottom)

FIGURE 7
Flow visualization results for 60° ribs with big gaps, $Re = 20{,}000$.

The Nusselt number distributions along the central lines (Center) of the rib-roughened and smooth side-walls are presented in Fig. 10. It is shown in this figure that after a short *Nu* deterioration at the inlet part of the test section, caused by the thermal boundary layer growth, the *Nu* turns into an increase, and

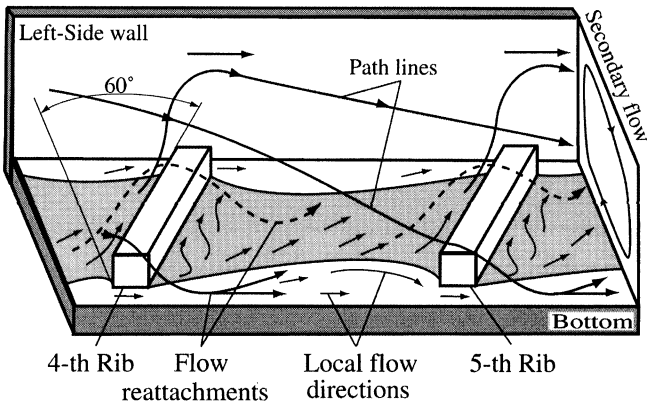

FIGURE 8
Flow pattern between 4th and 5th ribs with big gaps.

up-and-down fluctuation, which repeats correspondingly to the ribs positions. While in the case of NG this up-and-down fluctuation repeated in the entire test section, in the case of BG this phenomenon slowly changes with the distance from the inlet to the test section and development of the secondary flow and at around $z/d_e = 6$ it could be described only as a strong down-and-down *Nu* deterioration in the main flow direction. Despite this down-and-down deterioration, the *Nu* distribution for BG (●) is significantly higher than for the case of NG (■), especially at the end of the test section. The differences of the *Nu* distributions at the rib-roughened walls (● and ■) and smooth side-walls (□ and ○) can be also clearly observed.

Local Heat Transfer Distribution Under Rotation

Figure 11 shows the local Nusselt number distribution between the 7th and 8th ribs on the rib-roughened walls (Leading and Trailing walls) with the effects of rotation. It can be clearly seen from this figure that the rotation causes *Nu* enhancement

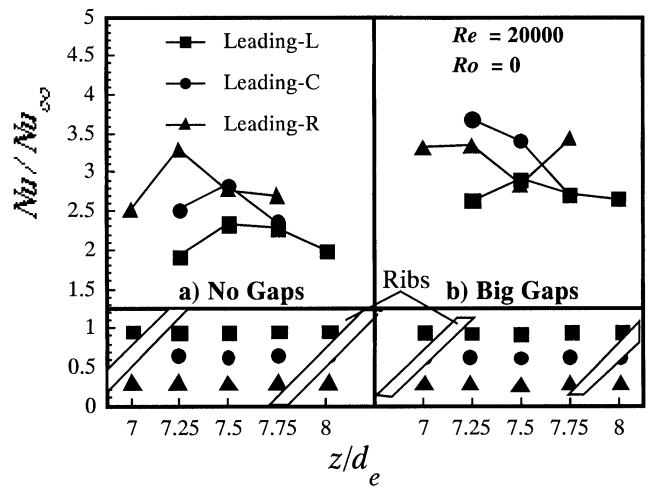

FIGURE 9
Local *Nu* distributions between 7th and 8th ribs for the stationary case.

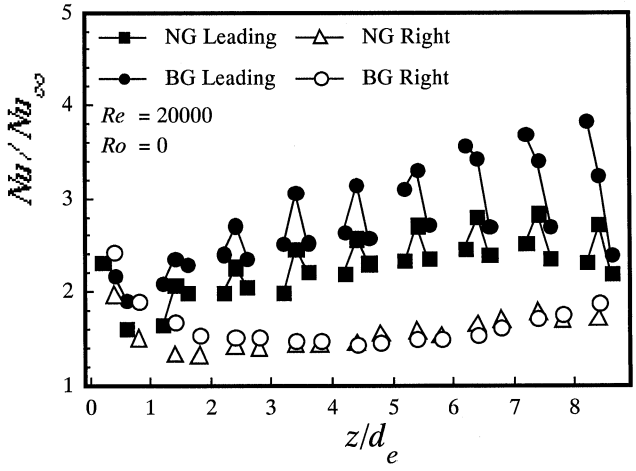

FIGURE 10
Nu distributions along the central lines of Leading and Right walls, $Ro = 0$.

on the Leading wall [(●), (■), (▲)] and a *Nu* deterioration on the Trailing wall [(△), (○), (□)] due to the development of an additional secondary flow induced by the Coriolis acceleration. This phenomenon strongly affects both rib configurations, but while in the case of the 60° ribs with No Gaps, this effect is limited, in the case of Big Gaps an appreciable *Nu* enhancement on the Leading wall is visible. The difference between the rib arrangements with No Gaps and Big Gaps for the stationary conditions, shown in the paragraph above, clearly enlarged under the rotating conditions. This fact can be also confirmed in closer look at the *Nu* distribution in the entire test section (see Figs. 12 and 13). As was noticed previously, the *Nu* at the inlet to the test section decreased in the entrance region of the test section due to the

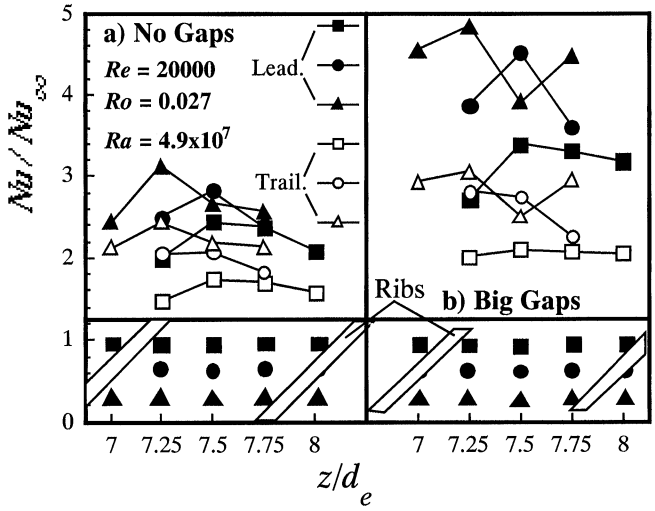

FIGURE 11
Local *Nu* distributions between 7th and 8th ribs for the rotating case.

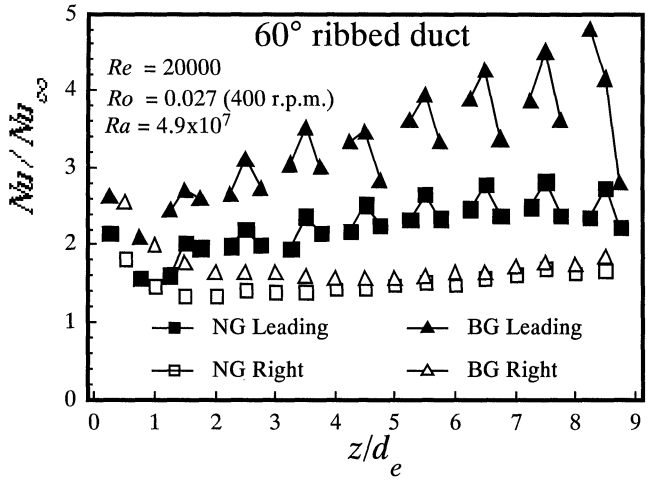

FIGURE 12
Nu distributions along the central lines of Leading and Right walls for No Gaps and Big Gaps, $Ro = 0.027$.

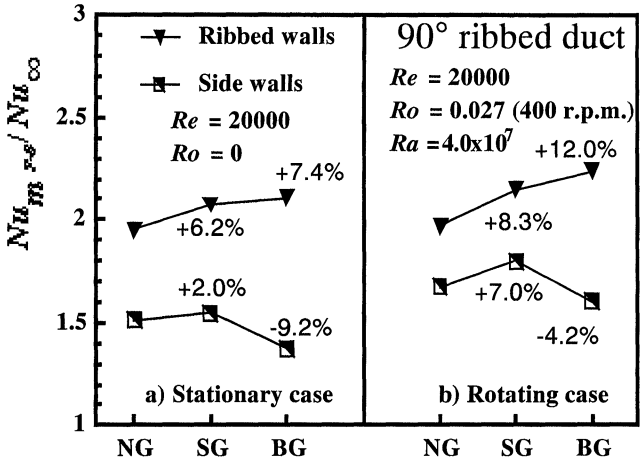

FIGURE 14
Mean *Nu* distributions between 7th and 8th 90° ribs for ribbed and smooth side walls.

boundary layer development. It rebounds at the area just after the first rib, and gradually increases with a development of the secondary flow caused by the 60° rib arrangements and Coriolis forces. The *Nu* in the case of Big gaps (▲) is higher in the entire test section than that of No Gaps (■). By comparing Figs. 10 and 12, one can see that the rotation magnifies the effects of the gaps on the heat transfer with the distance from the inlet to the test section.

The Nusselt number at the smooth side-walls, Right-side (□) and Left-side (△) walls respectively, shows only a small difference between both rib arrangements due to the creation of the fully developed turbulent profile and limited number of thermocouples.

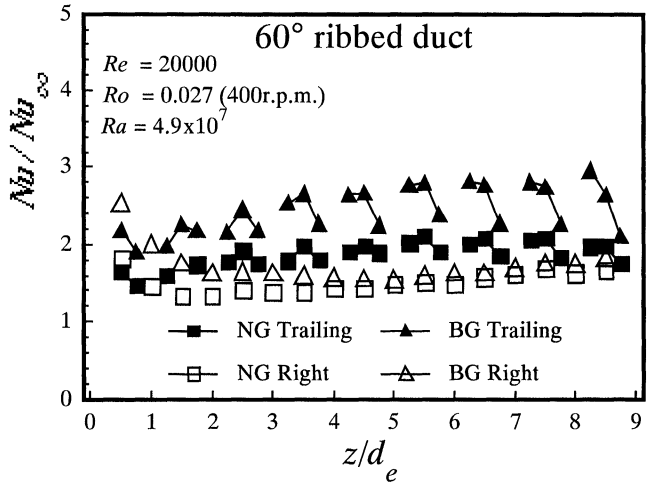

FIGURE 13
Nu distributions along the central lines of Trailing and Right walls for No Gaps and Big Gaps, $Ro = 0.027$.

Comparison Between 60° and 90° Rib Patterns

In Figs. 14 and 15, comparisons of the mean Nusselt numbers for the 90° and 60° ribs, N_{um7-8}, on the ribbed and smooth side-walls are made for the stationary and rotating cases. Figure 14 is used only for an assessment of the differences between the transverse and oblique ribs and it has been already published in Kiml et al. (2000).

By comparing these two figures one can clearly see that the gap effect on the mean Nusselt number between 7th and 8th ribs, N_{um7-8}, for the 60° rib arrangements is significantly stronger than in the case of the 90° rib arrangements. Particularly, the ribbed walls show almost 16% increase of the mean Nu_{m7-8}, if the Big Gaps are employed. This mean Nu_{m7-8} enhancement for

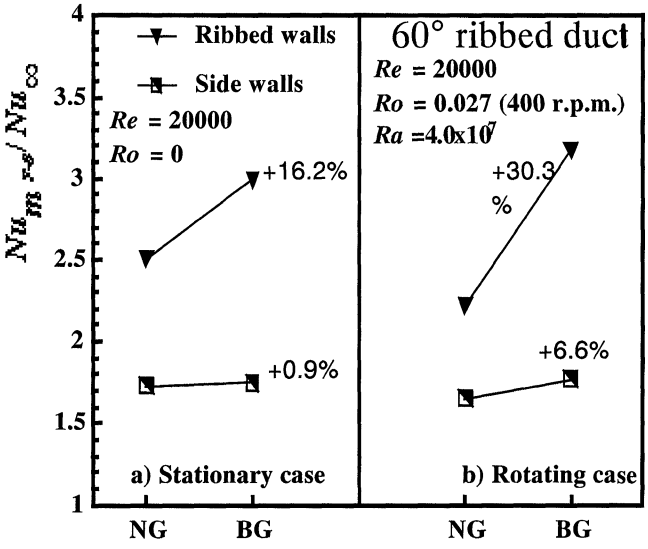

FIGURE 15
Mean *Nu* distributions between 7th and 8th 60° ribs for ribbed and smooth side walls.

the Big Gaps amplifies with the rotation up to 30% due to the secondary flow strengthened by the Coriolis forces. In contrast to the situation on the ribbed walls, the mean Nu_{m-8} on the smooth side-walls shows very similar values for both rib arrangements in the stationary case and only a small increase (6%) in the rotating case (the differences are within the uncertainty limit).

CONCLUSIONS

The flow visualization and heat transfer experiments were performed to examine the gap effects on the local heat transfer distribution between the consecutive ribs in a rib-roughened duct for the 60° ribs. Experiments were performed for the ribs mounted on two opposite sides of the duct for the following cases: (1) with No Gaps and (2) with Big Gaps = $1h$ between the side-walls and ribs. The heat transfer experiments were performed for both stationary and rotating cases and the flow visualization experiments only for the stationary case. The following conclusions were drawn:

1. The existence of the gaps between the 60° ribs and side-walls appreciably enhances the Nu on the ribbed walls inside a straight rib-roughened channel. It is caused by (a) the introduction of the fresh air through the gaps into the area between two consecutive ribs and (b) the improvement of the three-dimensional flow structure.
2. The Nusselt number enhancement on the ribbed walls caused by the existence of the gaps appreciably intensifies with the effects of rotation due to the development of an additional secondary flow induced by the Coriolis acceleration.
3. In contrast to the situation on the ribbed walls, the local Nusselt number on the smooth side-walls shows very similar values for both rib arrangements in the stationary case and only a small increase in the rotating case.
4. The mean Nusselt number between the 7th and 8th ribs for the 60° ribs, N_{um7-8}, is noticeably higher in comparison to that of the 90° ribs due to the development of the rib induced secondary flow, which carries the air from the channel core region towards the heated surface. This differences are especially obvious for the ribbed walls when the Big Gaps are employed due to the strengthening of the secondary flow by the Coriolis forces.

NOMENCLATURE

A_h	heat transfer surface area [m^2]
c_p	specific heat of air [J/kgK]
d_e	hydraulic diameter $(4ab/[2(a+b)])$, [m]
h	rib height [m]
k	air thermal conductivity [W/mK]
L	passage length [m]
$\dot{m}$	air mass flow rate [kg/s]
Nu	Nusselt number
Nu_∞	Nusselt number for fully developed flow in a smooth passage
Nu_{m7-8}	mean Nusselt number over the area between the 7th and 8th ribs
$\dot{q}_w$	wall heat flux [W/m^2]
$\dot{q}_{w7-8}$	wall heat flux between the 7th and 8th ribs [W/m^2]
Pr	Prandtl number of air
Ra	Rayleigh number
Re	Reynolds number
T_b	local bulk temperature [K], $(T_{in} + (z/L)(T_{out} - T_{in}))$
T_{in}	inlet bulk temperatures [K]
T_{out}	outlet bulk temperatures [K]
T_w	wall temperature [K]
u_m	air or water mean velocity [m/s]
w	channel width
z	distance from the entrance to the test section [m]
α	local heat transfer coefficient [W/m^{2}K]
ν	air or water kinematic viscosity [m^2/s]
β	air volumetric expansion coefficient [1/K]
ω	angular velocity of rotation [rad/s]

REFERENCES

Cheng, K. C., Shi, L., and Kurokawa, M., 1992, Visualization of Flow Patterns in a 180- Degree Sharp Turn of a Square Duct, *Proc. of 4th International Symposium on Transport Phenomena and Dynamics of Rotating Machinery*, USA, Hawaii, vol. A, pp. 124–132.

Cheng, K. C., and Shi, L., 1996, Visualization of Flow Patterns in a 90-Degree Sharp Turn of a Square Duct, *Proc. of 6th International Symposium on Transport Phenomena and Dynamics of Rotating Machinery*, USA, Hawaii, vol. 2, pp. 651–660.

Dutta, S., Han, J.-C., and Zhang, Y.-M., 1995, Influence of Rotation on Heat Transfer from a Two-Pass Channel with Periodically Placed Turbulence and Secondary Flow Promoters, *International Journal of Rotating Machinery*, vol. 1, pp. 129–144.

Dutta, S., Andrews, J. M., and Han, J.-C., 1996, Prediction of Turbulant Flow and Heat Transfer in Rotating Square and Rectangular Smooth Channels, *ASME Journal of Turbomachinery*, No. 96-GT-234.

Ekkad, S. V., and Han, J.-C., 1997, Detailed Heat Transfer Distribution in Two-Pass Square Channels with Rib Turbulators, *International Journal of Heat and Mass Transfer*, vol. 40, no. 11, pp. 2525–2537.

El-Husayni, H. A., Taslim, M. E., and Kercher, D. M., 1994. Experimental Heat Transfer Investigation of Stationary and Orthogonally Rotating Asymmetric and Symmetric Heated Smooth and Turbulated Channels, *Transactions of the ASME*, vol. 116, pp. 124–132.

Han, J. C., 1984, Heat Transfer and Friction in Channels with Two Opposite Rib-Roughened Walls, *ASME Journal of Heat Transfer*, vol. 106, pp. 774–781.

Han, J. C., Park, J. S., and Lei, C. K., 1985, Heat Transfer Enhancement in Channels with Rib Turbulence Promoters, *ASME Journal of Engineering for Gas Turbines and Power*, vol. 107, pp. 629–635.

Han, J. C., Zhang, Y. M., and Lee, C. P., 1991, Augmented Heat Transfer in Square Channels with Parallel, Crossed, and V-Shaped Angled Ribs, *ASME Journal of Heat Transfer*, vol. 113, pp. 590–596.

Han, J. C., and Zhang, Y. M., 1992, High Performance Heat Transfer Ducts with Parallel, Broken, and V-shaped ribs, *International Journal of Heat and Mass Transfer*, vol. 35, pp. 513–523.

Hirota, M., Fujita, H., Yokosawa, H., and Tanaka, Y., 1996, Characteristics of Turbulent Flow in a Rectangular Duct with Rib-Roughened Long-Side Walls, *Proc. of the 9th International Symposium on Transport Phenomena in Thermal-Fluids Engineering*, Singapore, June 25–28.

Hu, Z., and Shen, J., 1996, Secondary Flow and It's Contribution to Heat Transfer Enhancement in a Blade Cooling Passage with Discrete Ribs, *Proc. of International Gas Turbine and Aeroengine Congress & Exhibition Birmingham*, UK, June 10–13.

Johnson, B. V., Wagner, J. H., Steuber, G. D., and Yeh, F. C., 1993, Heat Transfer in Rotating Serpentine Passages with Selected Model Orientations for Smooth or Skewed Trip Walls, *ASME Paper* 93-GT-305.

Johnson, B. V., Wagner, J. H., Steuber, G. D., and Yeh, F. C., 1994, Heat Transfer in Rotating Serpentine Passages with Trips Skewed to the Flow, *ASME Journal of Turbomachinery*, vol. 116, pp. 113–123.

Kawaike, K., Anzai, S., Takehara, I., Sato, M., Matsuzaki, H., and Kobayashi, Y., 1995, Advanced Internal Cooling of Turbine Nozzles and Blades for 1500C-glass Gas Turbines, *Proc. of International Gas Turbine Congress*, Yokohama, Japan, October 22–27th 1995.

Kiml, R., Mochizuki, S., and Murata, A., 1998, Influence of 180 Degree Sharp Turn on the Heat Transfer and Flow Behavior in a Smooth Square Cross Sectional Serpentine Channel, 8th International symposium on Flow Visualization, *CD Rom Proc. of 8th International symposium on Flow Visualization*, Sorrento, Italy, Paper's File No. 067, pp. 1–8.

Kiml, R., Mochizuki, S., and Murata, A., 2000, Influence of the Gap Size between Side Walls and Ribs on the Heat Transfer in a Stationary and Rotating Straight Rib-Roughened Duct, *International Journal of Rotating Machinery*, vol. 6, no. 4, pp. 253–263.

Kiml, R., Mochizuki, S., and Murata, A., 2000, Function of Ribs as Turbulators and Secondary Flow Inducers, 9th International symposium on Flow Visualization, *CD Rom Proc. of 9th International symposium on Flow Visualization*, Edinburgh, United Kingdom, Paper's File No. 164, pp. 1–10.

Metzger, D. E., Plevich, C. W., and Fan, C. S., 1984, Pressure Loss Through Sharp 180 Degree Turn in Smooth Rectangular Channels, *Trans. ASME Journal of Engineering for Gas Turbines and Power*, vol. 106, pp. 677–681.

Mochizuki, S., Murata, A., and Fukunaga, M., 1997, Effects of Rib Arrangement on Pressure Drop and Heat Transfer in a Rib-roughened Channel with a Sharp 180° Turn, *ASME Journal of Turbomachinery*, vol. 119, pp. 610–616.

Mochizuki, S., Takamura, J., Yamawaki, S., and Yang, W. J., 1994, Heat Transfer in Serpentine Flow Passage with Rotation, *ASME Journal of Turbomachinery*, vol. 116, pp. 133–139.

Murata, A., Mochizuki, S., and Fukunaga, M., 1994, Detailed Measurement of Local Heat Transfer in a Square-Cross-Section Duct with a Sharp 180-deg Turn, *Proceedings of the 10th International Heat Transfer Conference*, Brighton, United Kingdom, vol. 4, pp. 291–296, Aug. 1994.

Rau, G., Cakan, M., Moeller, D., and Arts, T., 1996, The Effect of Periodic Ribs on the Local Aerodynamic and Heat Transfer Performance of a Straight Cooling Passage, *Proc. of International Gas Turbine and Aeroengine Congress & Exhibition Birmingham*, UK, June 10–13 1996.

Taslim, M. E., Rahman, A., and Spring, S. D., 1991, An Experimental Investigation of Heat Transfer Coefficients in a Spanwise Rotating Channel With Two Opposite Rib-Roughened Walls, *ASME Journal of Turbomachinery*, vol. 113, pp. 75–82.

Taslim, M. E., Li. T., and Kercher, D. M., 1994, Experimental Heat Transfer and Friction in Channels Roughened with Angled V shaped and discrete Ribs on Two Opposite Walls, *ASME Paper* 94-GT-163.

Wagner, J. H., Johnson, B. V., Graziani, R. A., and Ych, F. C., 1992, Heat Transfer in Rotating Serpentine Passages With Trips Normal to the Flow, *ASME Journal of Turbomachinery*, vol. 114, pp. 847–457.

Zhang, Y. M., Gu, W. Z., and Han, J. C., 1994, Heat Transfer and Friction in Rectangular Channels Ribbed and Ribbed-Grooved Walls, *ASME Journal of Heat Transfer*, vol. 116, pp. 58–65.